Enhanced degradation of sulfamethoxazole by peroxydisulfate activation with Mg-doped CuO

Jiajia Hao, Lan Xie, Yaxin Zhang, Shengtao Xing*

Hebei Key Laboratory of Inorganic Nanomaterials, College of Chemistry and Materials Science, Hebei Normal University, Shijiazhuang 050024, China, Tel. +86 311 80787400; Fax: +86 311 80787402; emails: stxing07@sina.com (S. Xing), 1325241628@qq.com (J. Hao), xl151311@163.com (L. Xie), 387576308@qq.com (Y. Zhang)

ABSTRACT

Mg-doped CuO samples were synthesized by a coprecipitation method and used for removing sulfamethoxazole with peroxydisulfate (PDS) activation. The doped Mg inhibited the growth of CuO crystal and led to the formation of nanoparticles with larger surface areas. In addition, the doped samples had high alkalinity and buffer capacity. Therefore, they exhibited much higher activity than pure CuO, and their performance was barely affected by the initial solution pH. The influences of catalyst and PDS dosages were also investigated. When 0.5 g L^{-1} of CuO–Mg and 0.25 mM of PDS were used, the consumption efficiency of PDS and the degradation efficiency of sulfamethoxazole reached 89% and 99.6%, respectively. The quenching experiments and electron paramagnetic resonance experiments indicated that $^\bullet SO_4^-$ and $^\bullet O_2^-$ should be the reactive species for sulfamethoxazole degradation. The doped Mg significantly promoted the production of $^\bullet SO_4^-$ and $^\bullet O_2^-$. Finally, the possible degradation pathway of sulfamethoxazole was discussed according to the liquid chromatography−mass spectrometry result.

Keywords: Mg-doped CuO; Peroxydisulfate; Sulfamethoxazole; Active radicals; Alkalinity

1. Introduction

The development of highly efficient technology for removing refractory organic pollutants has always been a hot topic in the field of water treatment. In recent years, persulfate, including peroxymonosulfate (PMS) and peroxydisulfate (PDS), activation processes have attracted great interest in removing pharmaceuticals because the formed sulfate radical ($^\bullet SO_4^-$) has higher oxidation ability, stability, and selectivity than hydroxyl radical ($^\bullet OH$) [1–7]. Among different activation processes, heterogeneous catalytic activation requires low-energy consumption and exhibits high performance in a wide pH range, thus receiving more attention. In comparison with PMS, PDS shows a better application potential due to its lower cost and higher stability [8–10].

Up to now, many efforts have been made to develop highly active catalysts for PDS activation, including metal, metal oxides, and carbonaceous materials [11–17]. Copper oxides were found to be effective for the removal of refractory organic pollutants. Various reactive oxygen species have been reported to be the dominant reactive species in the PDS activation processes with copper oxides. Accordingly, various activation mechanisms have also been proposed. It is well known that $^\bullet SO_4^-$ is the common reactive species and can be produced through the reaction of PDS with $\equiv Cu^{+/2+}$. The produced $^\bullet SO_4^-$ can react with OH^- to form hydroxyl radical ($^\bullet OH$). Our previous work found that $\equiv Cu^{2+}$ with more electron deficiency could promote the decomposition of PDS into superoxide radical ($^\bullet O_2^-$) [18,19]. In addition, CuO can activate PDS through the non-radical way [20–24]. The previous studies have demonstrated that the activation

* Corresponding author.

pathway and efficiency of PDS are dependent on the structure and property of copper oxides. Some methods, such as loading on support, doping, or compositing with other components, have been reported to be effective for improving the performance of a catalyst [11,12,25–36]. Among them, metal doping should be a simple and effective method for manipulating the performance of a catalyst. For instance, Zhou et al. [31] reported that the doping of nonreducible metal oxides onto $Cu@Fe_3O_4$ modified its surface properties and chemical state of Cu, thus, altering the activation pathway of PMS. Singlet oxygen ($^1O_2$) derived from the direct oxidation or the recombination of $\cdot O_2^-$ was the main reactive species in this process. Jawad et al. [32] also found that the incorporation of Mg oxide into CuO/Fe_3O_4 switched the radical activation process of PMS into the $^1O_2$ based non-radical process. Although PMS has a different structure and can be activated more readily compared to PDS, it can be deduced that the performance of CuO for PDS activation can be also affected by Mg doping.

Hence, in this work, Mg-doped CuO samples were synthesized by a facile coprecipitation method and investigated as a catalyst for PDS activation. Sulfamethoxazole is one of the widely used antibiotics in the world has been regularly detected in wastewater effluent, surface water, and drinking water (0.01–2.0 μg L^{-1}) [37]. Therefore, it was used as the target pollutant. The correlation between the surface properties and activities of the catalysts was analyzed by different characterization techniques. The possible mechanism for the enhanced performance of Mg-doped CuO was discussed. The influence of reaction parameters on its performance was investigated. Finally, the dominant reactive species for sulfamethoxazole removal and the possible degradation pathway of sulfamethoxazole were analyzed.

2. Experimental

2.1. Catalyst preparation

Pure CuO was prepared by a precipitation method. First, 1.025 g of $CuCl_2 \cdot 2H_2O$ was dissolved in distilled water. Then 1.5 mL of 8 M NaOH solution was added dropwise. The resultant suspension was magnetically stirred for 0.5 h and then allowed standing for 12 h. The precipitate was collected by the filtration and washed with ethanol and water. Finally, it was dried at 110°C for 6 h and calcined at 350°C for 4 h. Mg-doped samples were prepared by the same method except for the addition of $MgCl_2 \cdot 6H_2O$. The samples prepared with the Cu:Mg ratios of 20:1, 15:1, and 9:1 were designated as CuO-Mg1, CuO-Mg2, and CuO-Mg3, respectively. For comparison, Mg/CuO nanocomposites with the Cu:Mg ratios of 6:1 and 3:1 were also prepared and named as CuO-Mg4 and CuO-Mg5.

2.2. Catalyst characterization

The crystal phase and morphology of the prepared samples were examined by a Bruker D8-Advance powder X-ray diffractometer (XRD) and a Hitachi S-4800 field emission scanning electron microscope (SEM), respectively. The surface areas of the samples were determined by a Quantachrome NOVA 4000e surface area analyzer. The surface chemical state was measured by a Thermo

ESCALAB 250 X-ray photoelectron spectrometer (XPS). The isoelectric point of the sample was measured by the pH drift method. The content of CuO in the doped samples was determined by a Hitachi 180-70 atomic absorption spectrometer. These samples were dissolved with H_2SO_4 solution. The ratios of Cu to Mg in the final samples were proportional to their precursors, suggesting that the applied Mg in the source materials has entered the final catalysts.

2.3. Degradation of sulfamethoxazole by PDS activation with different samples

Catalytic tests were performed in a 200 mL glass beaker. In a typical experiment, a certain amount of $Na_2S_2O_8$ was added in 100 mL sulfamethoxazole solution (39.5 μM, 10 mg L^{-1}). The initial solution pH was adjusted to 8 using diluted NaOH solution. The reaction was started by adding 0.05 g of catalyst. At different reaction times, samples were withdrawn and filtered for analysis. The residue PDS in the solution was removed by $Na_2S_2O_3$ solution. The concentration of sulfamethoxazole was determined by a high-performance liquid chromatograph (HPLC, Agilent 1200) equipped with a ZORBAX Eclip se XDB-C18 column. Acetonitrile and ammonium acetate (1 mM) aqueous solution were used as the mobile phase. The degradation products were identified by a 3200 Q-TRAP liquid chromatograph-mass spectrometry (LC-MS, AB SCIEX). The consumption rates of PDS by different catalysts were determined by the potassium iodide method. The signals of 5,5-dimethy-1-pyrroline-N-oxide (DMPO) adducts with radicals in different catalytic processes were analyzed by a Magnettech MS-5000 electron paramagnetic resonance (EPR) spectrometer.

3. Results and discussion

3.1. Characterization of different samples

The crystal phase of the prepared samples was examined by the XRD analysis. As shown in Fig. 1, all the peaks
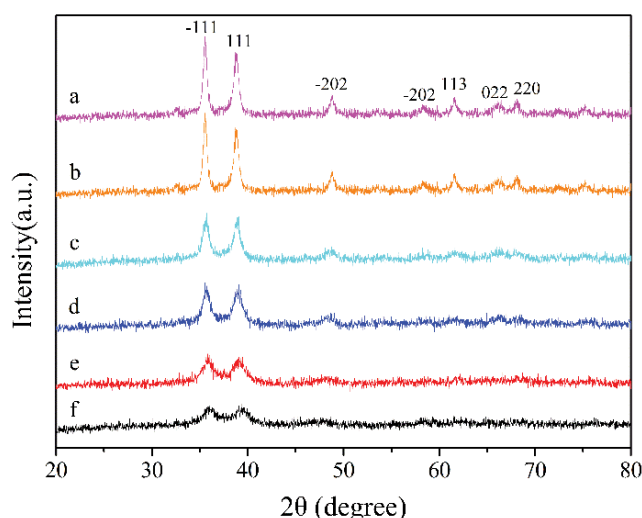

Fig. 1. XRD patterns of (a) CuO, (b) CuO-Mg1, (c) CuO-Mg2, (d) CuO-Mg3, (e) CuO-Mg4 and (f) CuO-Mg5.

of the samples can be indexed to monoclinic CuO crystal (JCPDS 80-1268), and the peak intensity decreased with increasing the content of Mg. The result indicates that the undoped sample is pure CuO. The lattice parameters of CuO are $a = 0.4676$, $b = 0.3418$, $c = 0.5129$ nm, and $\beta = 99.54°$. They all decreased after the doping of Mg. However, no peaks assigned to other components were observed for the other samples, which can be attributed to the low content and/or amorphous structure of Mg oxide. The weaker and wider peaks indicate the lower content and smaller crystal size of CuO. Mg might inhibit the crystallization of CuO and decrease its crystal size, which can be demonstrated by the morphology observation of these samples.

Fig. 2 shows the SEM images of different samples. The morphology of the pure CuO sample is irregular nanosheet. This is in accordance with the reported literature, and CuO nanosheets can be usually obtained by the dropwise addition of NaOH solution [38]. Interestingly, some nanosized particles were observed after doping a small amount of Mg (Fig. 2b), and their amount increased with increasing the content of doped Mg. When the Cu:Mg ratio was decreased to 9:1, nanosheets completely disappeared and the sample was composed of nanoparticles with sizes of several tens of nm. The smaller particle sizes of the doped samples are consistent with their XRD analysis result. In general, nanosized particles usually have large surface areas. The surface area of CuO is only 15 m^2 g^{-1}, and the doped samples have much larger surface areas due to their smaller particle sizes. The surface areas of CuO-Mg1, CuO-Mg2, CuO-Mg3, CuO-Mg4, and CuO-Mg5 were determined to be about 59, 79, 85, 96, and 129 m^2 g^{-1}, respectively. The incorporation of Mg inhibited the growth of CuO crystal and led to the formation of smaller particles. The isoelectric point of pure CuO was determined to be around 7, which is in accordance with the reported CuO samples in previous literature [21]. The surface chemical state of CuO and CuO-Mg3 was measured by XPS. As shown in Fig. 3, the binding energy of Cu 2p3/2 is 933.3 eV for pure CuO, which can be assigned to Cu^{2+}. In comparison with CuO, the Cu 2p3/2 peak of CuO-Mg3 shifted positively. This can be

attributed to the doping of Mg. The characterization results show that the structure of CuO was successfully modified through the incorporation of magnesium oxide, which might affect its activity for PDS activation.

3.2. Degradation of sulfamethoxazole by PDS activation with different samples

Fig. 4a shows the degradation of sulfamethoxazole by PDS activation with different samples. Sulfamethoxazole cannot be degraded by single PDS and PDS + MgO. The addition of CuO significantly accelerated its degradation. But its degradation efficiency was only 57.8% at a reaction time of 30 min. It is interesting that the activity of CuO was dramatically enhanced through the incorporation of Mg. The activity of these samples was positively correlated with the content of Mg, but its effect was limited. CuO-Mg3, CuO-Mg4, and CuO-Mg5 exhibited similar
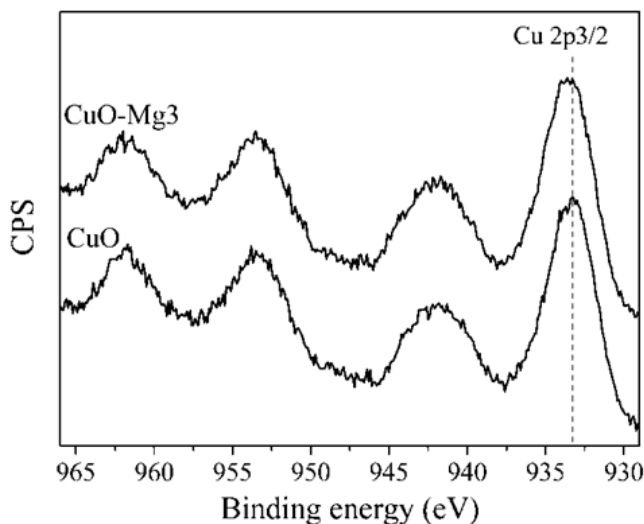

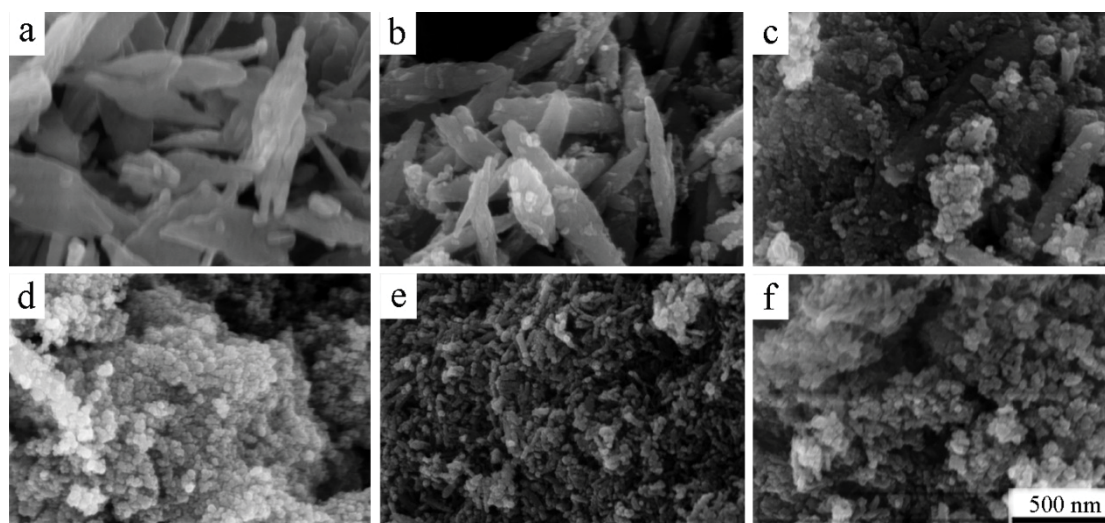Fig. 3. Cu 2p XPS spectra of CuO and CuO-Mg3.

Fig. 2. SEM images of (a) CuO, (b) CuO-Mg1, (c) CuO-Mg2, (d) CuO-Mg3, (e) CuO-Mg4 and (f) CuO-Mg5.
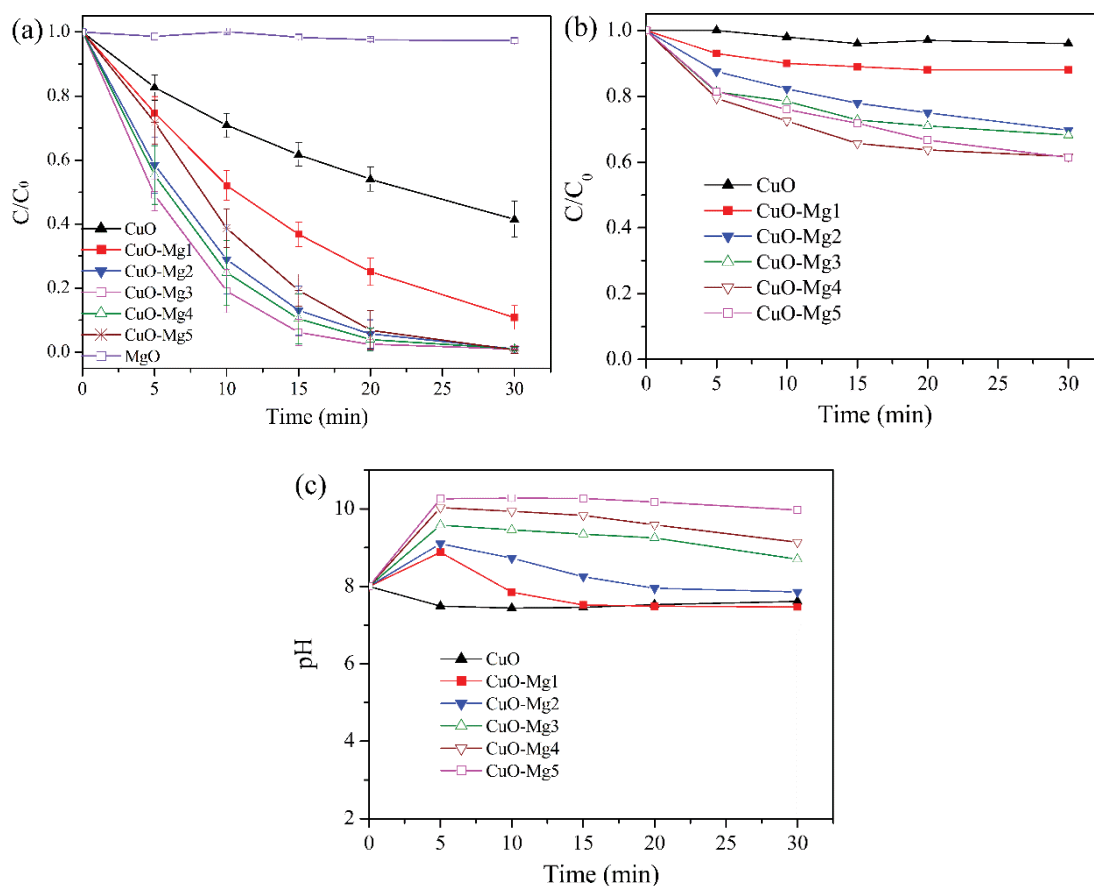
Fig. 4. Sulfamethoxazole degradation (a), PDS consumption (b), and pH changes (c) in different PDS activation processes (initial pH 8, catalyst 0.5 g L^{-1}, PDS 1 mM).

activity for sulfamethoxazole degradation, and more than 97% of sulfamethoxazole was degraded within 15 min. In general, the degradation efficiency of pollutant was mainly dependent on the activation efficiency of PDS. Fig. 4b shows the consumption efficiencies of PDS by different samples. The result is consistent with the activity of these samples for sulfamethoxazole degradation. This means that more reactive species might be produced from the decomposition of PDS, thus, promoting the degradation of sulfamethoxazole. The doped samples have much larger surface areas, which can provide much more active sites for the decomposition of PDS into reactive species. In addition, the activation efficiency of PDS is tightly associated with the solution pH and PDS is readily decomposed at higher pH. Fig. 4c shows the change of solution pH after the addition of different samples into the sulfamethoxazole-PDS solution. The solution pH decreased slightly with the addition of CuO, while that in the presence of Mg incorporated samples all increased at the initial stage. The pH values in different systems were positively correlated with the content of Mg, which can be due to its high alkalinity and buffer capacity. It is well known that the higher solution pH facilitates the decomposition of PDS. Therefore, the doped samples exhibited higher activity for PDS decomposition than pure CuO. The performance of CuO for the degradation of sulfamethoxazole at pH 10 was also examined. As shown in Fig. 5a, 89.6% of sulfamethoxazole was degraded by CuO at pH 10, much higher than that by CuO at pH 8. However, the activity of CuO at pH 10 was still much lower than those of CuO-Mg. This could be attributed to the larger surface areas of CuO-Mg. Because the CuO-Mg samples have higher surface areas and buffer capacity, they exhibited higher activity for the activation of PDS and the degradation of sulfamethoxazole.

It is worth pointing out that all the samples exhibited poor adsorption capacity towards sulfamethoxazole and the maximum adsorption rate was only 2.1%. This may be caused by the electrostatic repulsion between sulfamethoxazole and catalyst surface. Because the pKa value of sulfamethoxazole is 5.6 and the isoelectric point of CuO is about 7, they are both negatively charged at initial pH 8 [39]. Moreover, the solution pH further increased with the addition of Mg incorporated samples, and the electrostatic repulsion might be also enhanced. Therefore, although Mg incorporated samples have much larger surface areas than pure CuO, they still exhibited very low adsorption capacities towards sulfamethoxazole. Because the introduced Mg increased the solution pH, the leaching of Cu was significantly hindered. The maximum concentration of leached Cu in the CuO-Mg-PDS process was only 0.028 mg L^{-1}, much lower than that in the CuO-PDS process (0.726 mg L^{-1}). Accordingly, the contribution of homogeneous reactions to

pollutant removal can be ignored. In addition, the incorporation of magnesium oxide should be an efficient method to avoid the secondary pollution of Cu leaching.

3.3. Influence of reaction conditions on catalytic performance of CuO-Mg

The above results demonstrate that the incorporation of Mg successfully improved the catalytic performance of CuO. Subsequently, the influence of reaction conditions on the performance of CuO-Mg was further studied. Fig. 5a shows the degradation of sulfamethoxazole with CuO-Mg3 at different initial pH. Initial solution pH had a slight effect on sulfamethoxazole degradation, and the degradation rate was accelerated with increasing pH. This can be ascribed to the high buffer capacity of CuO-Mg. Although the initial pH values were quite different, they became similar after the addition of CuO-Mg. Our previous work has found that the initial solution pH had a stronger effect on pure CuO. Moreover, the leaching of Cu was serious at low pH [20]. As for CuO-Mg, it showed high activity in a wide pH range, and the leaching of Cu was also avoided even when the target pollutant solution was acidic.

Fig. 5b shows the degradation of sulfamethoxazole with different PDS concentrations. Sulfamethoxazole cannot be degraded in the absence of PDS, and only 2% of

sulfamethoxazole was adsorbed on CuO-Mg. The addition of a small amount of PDS (0.25 mM) significantly increased the degradation efficiency to 99.6% within 30 min. The degradation rate was further accelerated by increasing the concentration of PDS. For instance, the degradation efficiency at 5 min was increased from 65.6% to 96.3% by increasing the concentration of PDS from 0.25 to 10 mM. This can be ascribed to the formation of more reactive species at a higher PDS concentration, resulting in the faster degradation of sulfamethoxazole.

Fig. 5c shows the influence of CuO-Mg dosage on this process. Only 3% of sulfamethoxazole was degraded at pH 8 in the absence of CuO-Mg, and the degradation efficiency was slightly increased to 3.8% by increasing the initial pH to 10. It can be seen that sulfamethoxazole was almost completely removed at a reaction time of 30 min by the addition of 0.5 g L^{-1} of CuO-Mg. The degradation rate increased gradually with an increasing catalyst dosage from 0.5 to 3 g L^{-1}. But the further increase of catalyst dosage had little effect on the degradation of sulfamethoxazole. It is well known that more active sites can be provided for the production of more reactive species at a higher catalyst concentration. However, the catalyst aggregation will also occur, and the formed radicals can also be consumed by the excessive catalyst. Thus, the optimized catalyst dosage should be 3 g L^{-1} in terms of pollutant degradation
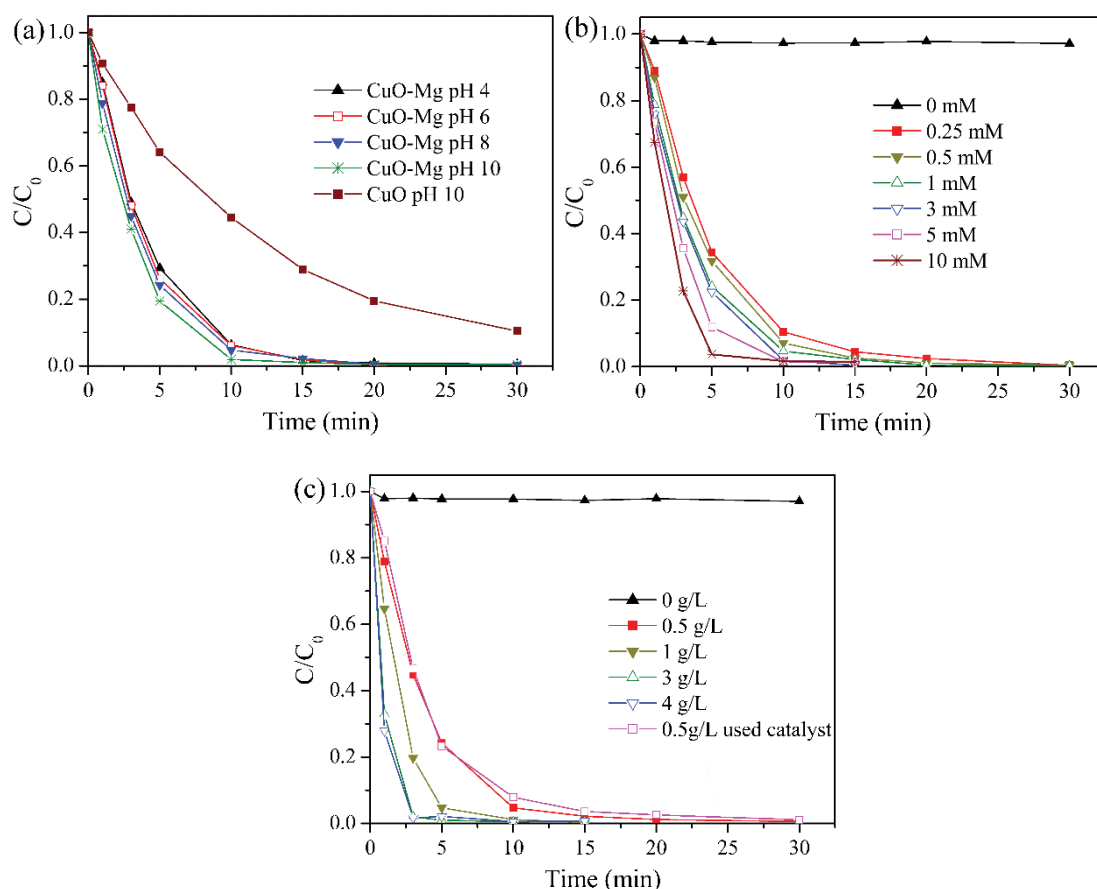

Fig. 5. Effect of initial solution pH (a), PDS concentration (b), and catalyst dosage (c) on sulfamethoxazole degradation with CuO-Mg3 (initial pH 8, catalyts 0.5 g L^{-1}, PDS 1 mM).

rate. In addition, the used catalysts were recovered by centrifugation and reused without any treatment. It still exhibited high activity for sulfamethoxazole degradation, demonstrating its good reusability.

Although pollutants can be degraded rapidly at a high PDS concentration, the utilization rate of PDS is usually low. As shown in Fig. 6, only 31.8% of PDS was consumed within 30 min at a concentration of 1 mM. When the concentration of PDS was decreased to 0.25 mM, the consumption efficiency of PDS was increased to 89%. Moreover, sulfamethoxazole can also be completely removed using 0.25 mM PDS (Fig. 5b). The reaction stoichiometric efficiency (RSE, the mole ratio of degraded sulfamethoxazole to consumed PDS) is an important parameter for the assessment of PDS activation processes. It was calculated to be 13.5% for 1 mM PDS. When the PDS concentration was 0.25 mM, the RSE was 17.7%, much higher than many reported chemically activated PDS processes [40–45], demonstrating the potential application of this catalyst. In addition, CuO-Mg was also compared with some reported catalysts for the degradation of sulfamethoxazole (Table 1), and it exhibited relatively higher activity [26,45–48].

Some substances in real water usually compete for active species and inhibit the degradation of target pollutants.
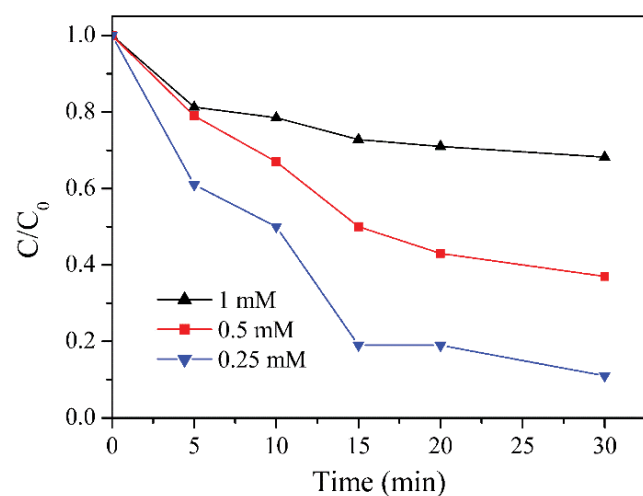
Therefore, the degradation of sulfamethoxazole in the presence of different coexisting substances was further investigated. As shown in Fig. 7, fulvic acid, bicarbonate, and chloride ions all hindered the degradation of sulfamethoxazole to some extent. Fulvic acid is a common organic matter in water and can react with many reactive species, while bicarbonate and chloride ions are effective scavengers of active radicals [49,50]. The result indicates that this process might follow a radical mechanism.

3.4. Active species for the degradation of sulfamethoxazole with CuO-Mg

It is well known that $^\bullet SO_4^-$ can be generated through the activation of PDS [Eqs. (1) and (2)] and it can react with OH^- to form hydroxyl radical ($^\bullet OH$). Our previous work found that $^\bullet O_2^-$ can also be generated from PDS activation [Eqs. (3) and (4)] [20,21]. In addition, some literatures reported that $^1O_2$ was the reactive species for pollutants degradation and can be generated by direct oxidation or recombination of $^\bullet O_2^-$ [32,51]. Ethanol (EtOH), tert-butanol (TBA), *p*-benzoquinone (BQ), and NaN_3 are widely used scavengers for the identification of $^\bullet SO_4^-$, $^\bullet OH$, $^\bullet O_2^-$ and

Fig. 6. Effect of PDS concentration on its consumption rate with CuO-Mg3 (initial pH 8, catalyst 0.5 g L^{-1}).
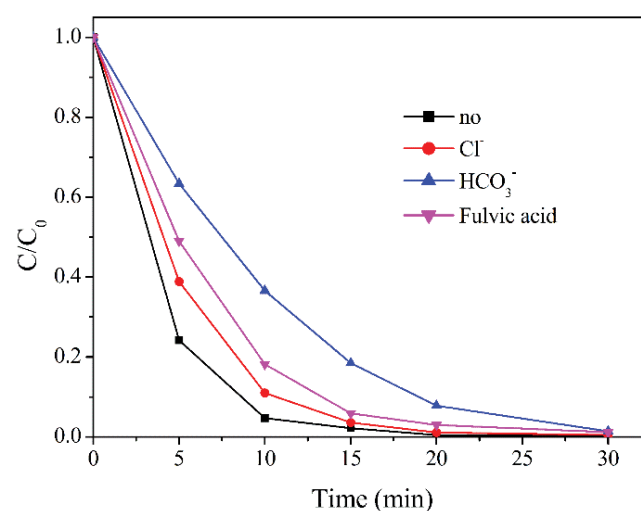

Fig. 7. Effect of coexisting substances on sulfamethoxazole degradation with CuO-Mg3 (initial pH 8, catalyst 0.5 g L^{-1}, PDS 1 mM, fulvic acid 10 mg L^{-1}, Cl$^-$ and HCO$_3^-$ 500 mM).

Table 1
Comparison of different PDS or PMS activation processes for sulfamethoxazole removal

Catalyst	C_0	PDS or PMS concentration	Catalyst dosage	Reaction time	Removal rate	References
CuO-Mg	10 mg/L	0.25 mM	0.5 g/L	30 min	99.6%	This work
TiO$_{2-x}$/rGO + Vis	10 mg/L	2 mM	1 g/L	40 min	52%	[46]
CuO@Al$_2$O$_3$	10 mg/L	0.4 mM	0.5 g/L	120 min	99%	[26]
N-doped graphene	5 mg/L	1 mM	0.05 g/L	180 min	>99%	[47]
UV$_{254}$	20 μm	1 mM	–	120 min	100%	[37]
Micrometric Fe^0	10 mg/L	1 mM	0.125 g/L	120 min	95%	[42]
Fe$_3$O$_4$/β-FeOOH	5 mg/L	0.15 g/L	0.2 g/L	30 min	91%	[48]

$^1O_2$, respectively. Their effect on sulfamethoxazole degradation is presented in Fig. 8. TBA and NaN_3 did not affect this process, indicating that the contribution of $^\bullet OH$ and $^1O_2$ can be excluded. In comparison with TBA, EtOH has a much higher rate constant with $^\bullet SO_4^-$ and its addition significantly suppressed the degradation of sulfamethoxazole. This means that $^\bullet SO_4^-$ played an important role in this process. In addition, the addition of BQ also showed a strong inhibitory effect. Accordingly, both $^\bullet SO_4^-$ and $^\bullet O_2^-$ should be the reactive species for sulfamethoxazole degradation. However, the degradation could not be completely inhibited when ethanol or BQ was added. According to previous literatures, CuO is also an effective catalyst for non-radical activation of PDS [20–24]. It can be deduced that the activated PDS generated from the non-radical pathway might also participate in the degradation of sulfamethoxazole.
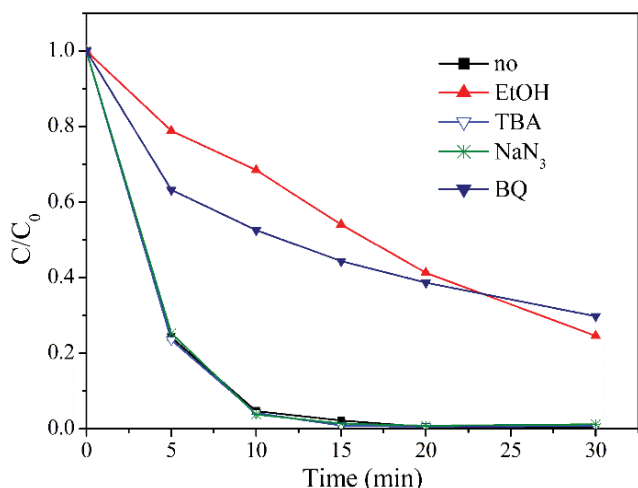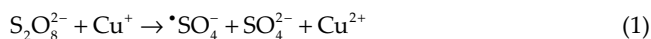
$$S_2O_8^{2-} + Cu^+ \rightarrow {}^\bullet SO_4^- + SO_4^{2-} + Cu^{2+} \tag{1}$$

Fig. 8. Effect of scavengers on sulfamethoxazole degradation with CuO-Mg3 (initial pH 8, catalyst 0.5 g L^{-1}, PDS 1 mM, BQ 1 mM, NaN_3 5 mM, TBA and EtOH 500 mM).
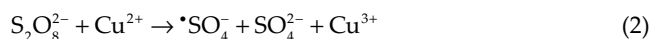
$$S_2O_8^{2-} + Cu^{2+} \rightarrow {}^\bullet SO_4^- + SO_4^{2-} + Cu^{3+} \tag{2}$$

$$\equiv Cu^{2+} \cdots S_2O_8^{2-} + 2H_2O \rightarrow 2HSO_4^- + {}^\bullet O_2^- + 2H^+ \tag{3}$$

$$\equiv Cu^{3+} \cdots S_2O_8^{2-} + 2H_2O \rightarrow 2HSO_4^- + {}^\bullet O_2^- + 2H^+ \tag{4}$$

Fig. 9a shows the signals of $^\bullet SO_4^-$–DMPO and $^\bullet OH$–DMPO in the aqueous PDS solution with CuO and CuO-Mg. No signals can be observed for CuO, while the signals of $^\bullet SO_4^-$–DMPO and $^\bullet OH$–DMPO were both observed for CuO-Mg. The weak signals of $^\bullet SO_4^-$–DMPO compared to $^\bullet OH$–DMPO are due to its low sensitivity. Because $^\bullet O_2^-$ has much lower reactivity toward DMPO than $^\bullet SO_4^-$ and $^\bullet OH$, its determination was carried out in a methanol/water (9:1) mixed solution. As shown in Fig. 9b, the signal of $^\bullet O_2^-$ DMPO was observed in the two systems, indicating that $^\bullet O_2^-$ can be generated by PDS activation with CuO. The signal intensity in the CuO-Mg system was much stronger than that in the CuO system. The results in Fig. 9a and b indicate that more $^\bullet SO_4^-$, $^\bullet OH$ and $^\bullet O_2^-$ can be generated by CuO-Mg. Since the contribution of $^\bullet OH$ has been excluded in Fig. 8, and sulfamethoxazole should be mainly degraded by $^\bullet SO_4^-$ and $^\bullet O_2^-$. The enhanced degradation of sulfamethoxazole by CuO-Mg could be attributed to its high activity for PDS activation. In comparison with CuO, CuO-Mg has a much higher surface area, alkalinity, and buffer capacity, and so it can promote the formation of more $^\bullet SO_4^-$ and $^\bullet O_2^-$ from PDS decomposition.

Finally, the degradation products of sulfamethoxazole were determined by the LC-MS. As shown in Table 2, sulfamethoxazole should be degraded through the cleavage of the N–S bond, leading to the formation of P2 [37]. P2 was further degraded into P4, P5, and P6 due to the cleavage of the oxazole ring. P1 was formed due to the oxidation of the substituent groups on the benzene ring. The benzene ring of P1 was further attacked by reactive radicals, resulting in the production of P3 and P4. The dominant degradation products were small molecular carboxylic acids. The total organic carbon removal rate was determined to be 53%
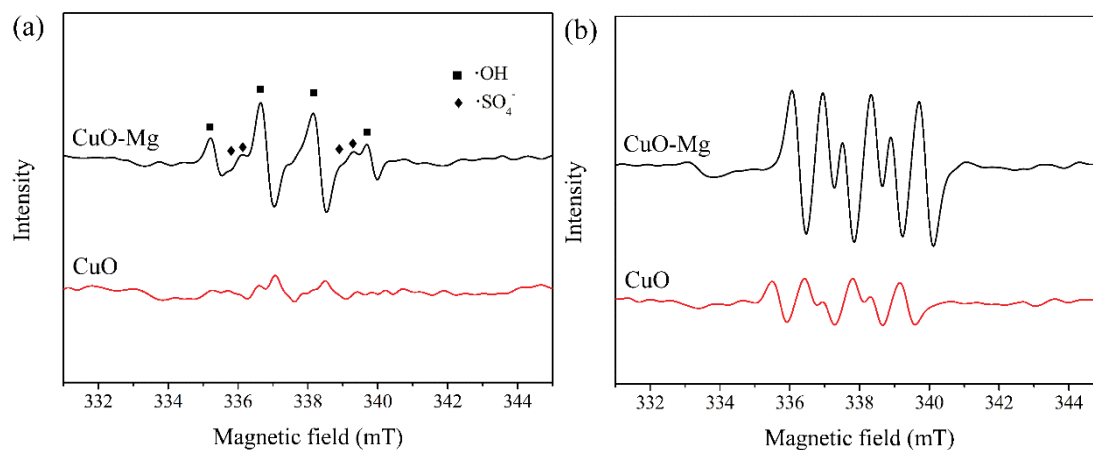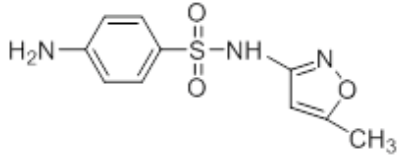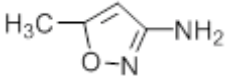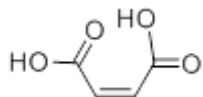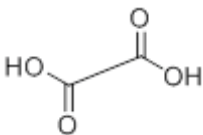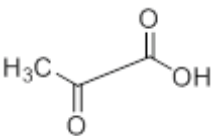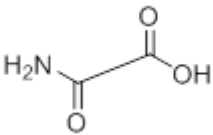

Fig. 9. EPR signals of (a) $^\bullet SO_4^-$–DMPO, $^\bullet OH$–DMPO, and (b) $^\bullet O_2^-$–DMPO in CuO and CuO-Mg PDS activation processes (initial pH 8, catalyst 0.5 g L^{-1}, PDS 1 mM, DMPO 100 μM).

Table 2
Identified organic products in the CuO-Mg-PDS process

Products	m/z	Chemical structure
Sulfame-thoxazole	253	
P1	108	
P2	98	
P3	116	
P4	90	
P5	88	
P6	89	

with 0.5 g L^{-1} CuO-Mg and 1 mM PDS, demonstrating that CuO-Mg-PDS is an effective technology for the deep oxidation of sulfamethoxazole.

4. Conclusion

Mg-doped CuO samples were successfully synthesized by a coprecipitation method and exhibited much higher activity than pure CuO for removing sulfamethoxazole with PDS activation. The doped samples have larger surface areas, higher alkalinity, and buffer capacity, and so can promote the formation of $^\bullet SO_4^-$ and $^\bullet O_2^-$ for degrading sulfamethoxazole. Moreover, their performance was barely affected by the initial solution pH and the leaching of Cu was significantly suppressed. When the dosage of catalyst and PDS were 0.5 g L and 0.25 mM, sulfamethoxazole was almost completely removed and 89% of PDS was consumed. The common substances in real water only had a slight effect on this process. The dominant degradation products

of sulfamethoxazole were identified to be small molecular carboxylic acids by the LC-MS analysis. The results implied the potential application of CuO-Mg-PDS for removing organic pollutants in water.

References

[1] L.W. Matzek, K.E. Carter, Activated persulfate for organic chemical degradation: a review, Chemosphere, 151 (2016) 178–188.
[2] S. Wacławek, H.V. Lutze, K. Grübel, V.V. Padil, M. Černík, D.D. Dionysiou, Chemistry of persulfates in water and wastewater treatment: a review, Chem. Eng. J., 330 (2017) 44–62.
[3] I.A. Ike, K.G. Linden, J.D. Orbell, M. Duke, Critical review of the science and sustainability of persulphate advanced oxidation processes, Chem. Eng. J., 338 (2018) 651–669.
[4] J. Wang, S. Wang, Activation of persulfate (PDS) and peroxymonosulfate (PMS) and application for the degradation of emerging contaminants, Chem. Eng. J., 334 (2018) 1502–1517.
[5] F. Ghanbari, M. Moradi, Application of peroxymonosulfate and its activation methods for degradation of environmental organic pollutants: review, Chem. Eng. J., 310 (2018) 41–62.
[6] S. Nimai, H. Zhang, Z. Wu, N. Li, B. Lai, Efficient degradation of sulfamethoxazole by acetylene black activated peroxydisulfate, Chin. Chem. Lett., 31 (2020) 2657–2660.
[7] H. Zhang, Q. Ji, L. Lai, G. Yao, B. Lai, Degradation of p-nitrophenol (PNP) in aqueous solution by mFe/Cu-air-PS system, Chin. Chem. Lett., 30 (2019) 1129–1132.
[8] G.P. Anipsitakis, D.D. Dionysiou, Degradation of organic contaminants in water with sulfate radicals generated by the conjunction of peroxymonosulfate with cobalt, Environ. Sci. Technol., 37 (2003) 4790–4797.
[9] T.K. Lau, W. Chu, N.J. Graham, The aqueous degradation of butylated hydroxyanisole by UV/$S_2O_8^{2-}$: study of reaction mechanisms via dimerization and mineralization, Environ. Sci. Technol., 41 (2007) 613–619.
[10] J. Saien, Z. Ojaghloo, A. Soleymani, M. Rasoulifard, Homogeneous and heterogeneous AOPs for rapid degradation of Triton X-100 in aqueous media via UV light, nano titania hydrogen peroxide and potassium persulfate, Chem. Eng. J., 167 (2011) 172–182.
[11] A. Jawad, J. Lang, Z. Liao, A. Khan, J. Ifthikar, Z. Lv, S. Long, Z. Chen, Z. Chen, Activation of persulfate by CuOx@Co-LDH: a novel heterogeneous system for contaminant degradation with broad pH window and controlled leaching, Chem. Eng. J., 335 (2018) 548–559.
[12] Y. Lei, C.S. Chen, Y.J. Tu, Y.H. Huang, H. Zhang, Heterogeneous degradation of organic pollutants by persulfate activated by CuO-Fe$_3$O$_4$: mechanism, stability, and effects of pH and bicarbonate ions, Environ. Sci. Technol., 49 (2015) 6838–6845.
[13] Y. Wang, H. Sun, H.M. Ang, M.O. Tadé, S. Wang, Magnetic Fe$_3$O$_4$/carbon sphere/cobalt composites for catalytic oxidation of phenol solutions with sulfate radicals, Chem. Eng. J., 245 (2014) 1–9.
[14] X. Jiang, Y. Guo, L. Zhang, W. Jiang, R. Xie, Catalytic degradation of tetracycline hydrochloride by persulfate activated with nano Fe^0 immobilized mesoporous carbon, Chem. Eng. J., 341 (2018) 392–401.
[15] G. Zhang, Z. Wu, H. Liu, Q. Ji, J. Qu, J. Li, Photoactuation healing of α-FeOOH@g-C$_3$N$_4$ catalyst for efficient and stable activation of persulfate, Small, 13 (2017) 1702225.
[16] W. Ren, L. Xiong, X. Yuan, Z. Yu, H. Zhang, X. Duan, S. Wang, Activation of peroxydisulfate on carbon nanotubes: electron transfer mechanism, Environ. Sci. Technol., 53 (2019) 14595–14603.

[17] D. Ouyang, J. Yan, L. Qian, Y. Chen, L. Han, A. Su, W. Zhang, H. Ni, M. Chen, Degradation of 1,4-dioxane by biochar supported nano magnetite particles activating persulfate, Chemosphere, 184 (2017) 609–617.

[18] Q. Wang, B. Wang, Y. Ma, S. Xing, Enhanced superoxide radical production for ofloxacin removal via persulfate activation with Cu-Fe oxide, Chem. Eng. J., 354 (2018) 473–480.

[19] W. Li, Y. Wu, Y. Gao, S. Xing, Mechanism of persulfate activation with CuO for removing cephalexin and ofloxacin in water, Res. Chem. Intermed., 45 (2019) 5549–5558.

[20] W. Li, B. Liu, Y. Wu, Y. Gao, S. Xing, Removal of ciprofloxacin by persulfate activation with CuO: a pH-dependent mechanism, Chem. Eng. J., 382 (2020) 122837.

[21] B. Liu, Y. Li, S. Xing, Insight into the mechanism of CuO activated persulfate with the assistance of bicarbonate for removing organic pollutants, J. Water. Process. Eng., 37 (2020) 101403.

[22] T. Zhang, Y. Chen, Y. Wang, J.L. Roux, Y. Yang, J. Croué, Efficient peroxydisulfate activation process not relying on sulfate radical generation for water pollutant degradation, Environ. Sci. Technol., 48 (2014) 5868–5875.

[23] X. Du, Y. Zhang, I. Hussain, S. Huang, W. Huang, Insight into reactive oxygen species in persulfate activation with copper oxide: activated persulfate and trace radicals, Chem. Eng. J., 313 (2017) 1023–1032.

[24] X. Du, Y. Zhang, F. Si, C. Yao, M. Du, I. Hussain, H. Kim, S. Huang, Z. Lin, W. Hayat, Persulfate non-radical activation by nano-CuO for efficient removal of chlorinated organic compounds: reduced graphene oxide-assisted and CuO (001) facet-dependent, Chem. Eng. J., 356 (2019) 178–189.

[25] S. Guo, Y. Jiang, L. Li, X. Huang, Z. Zhuang, Y. Yu, Thin CuO*x*-based nanosheets for efficient phenol removal benefitting from structural memory and ion exchange of layered double oxides, J. Mater. Chem. A, 6 (2018) 4167–4178.

[26] J.F. Yan, J. Li, J.L. Peng, H. Zhang, Y.H. Zhang, B. Lai, Efficient degradation of sulfamethoxazole by the CuO@Al$_2$O$_3$ (EPC) coupled PMS system: optimization, degradation pathways and toxicity evaluation, Chem. Eng. J., 359 (2019) 1097–1110.

[27] X. Zhang, M. Feng, L. Wang, R. Qu, Z. Wang, Catalytic degradation of 2-phenylbenzimidazole-5-sulfonic acid by peroxymonosulfate activated with nitrogen and sulfur co-doped CNTs-COOH loaded CuFe$_2$O$_4$, Chem. Eng. J., 307 (2017) 95–104.

[28] Y. Li, L. Guo, D. Huang, A. Jawad, Z. Chen, J. Yang, W. Liu, Y. Shen, M. Wang, G. Yin, Support-dependent active species formation for CuO catalysts: leading to efficient pollutant degradation in alkaline conditions, J. Hazard. Mater., 328 (2017) 56–62.

[29] Y. Liu, W. Guo, H. Guo, X. Ren, Q. Xu, Cu(II)-doped V$_2$O$_5$ mediated persulfate activation for heterogeneous catalytic degradation of benzotriazole in aqueous solution, Sep. Purif. Technol., 230 (2020) 115848.

[30] M. Sun, Y. Lei, H. Cheng, J. Ma, Y. Qin, Y. Kong, S. Komarneni, Mg-doped CuO-Fe$_2$O$_3$ composites activated by persulfate as highly active heterogeneous catalysts for the degradation of organic pollutants, J. Alloys Compd., 825 (2020) 154036.

[31] X. Zhou, A. Jawad, M. Luo, C. Luo, T. Zhang, H. Wang, J. Wang, S. Wang, Z. Chen, Z. Chen, Regulating activation pathway of Cu/persulfate through the incorporation of unreducible metal oxides: pivotal role of surface oxygen vacancies, Appl. Catal. B, 286 (2021) 119914.

[32] A. Jawad, K. Zhan, H. Wang, A. Shahzad, Z. Zeng, J. Wang, X. Zhou, H. Ullah, Z. Chen, Z. Chen, Tuning of persulfate activation from a free radical to a nonradical pathway through the incorporation of non-redox magnesium oxide, Environ. Sci. Technol., 54 (2020) 2476–2488.

[33] K. Salehi, B. Shahmoradi, A. Bahmani, M. Pirsaheb, H.P. Shivaraju, Optimization of reactive black 5 degradation using hydrothermally synthesized NiO/TiO$_2$ nanocomposite under natural sunlight irradiation, Desal. Water. Treat., 57 (2016) 25256–25266.

[34] R. Ebrahimi, K. Hossienzadeh, A. Maleki, R. Ghanbari, R. Rezaee, M. Safari, B. Shahmoradi, H. Daraei, A. Jafari, K. Yetilmezsoy, S.H. Puttaiah, Effects of doping zinc oxide nanoparticles with transition metals (Ag, Cu, Mn) on photocatalytic degradation of Direct Blue 15 dye under UV and visible light irradiation, J. Environ. Health. Sci., 17 (2019) 479–492.

[35] B. Vakili, B. Shahmoradi, A. Maleki, M. Safari, J. Yang, R.R. Pawar, S.M. Lee, Synthesis of immobilized cerium doped ZnO nanoparticles through the mild hydrothermal approach and their application in the photodegradation of synthetic wastewater, J. Mol. Liq., 280 (2019) 230–237.

[36] B. Shahmoradi, M. Pirsaheb, M.A. Pordel, T. Khosravi, R.R. Pawar, S. Lee, Photocatalytic performance of chromium-doped TiO$_2$ nanoparticles for degradation of Reactive Black 5 under natural sunlight illumination, Desal. Water. Treat., 67 (2017) 324–331.

[37] Y. Yang, X. Lu, J. Jiang, J. Ma, G. Liu, Y. Cao, W. Liu, J. Li, S. Pang, X. Kong, C. Luo, C. Degradation of sulfamethoxazole by UV, UV/H$_2$O$_2$ and UV/persulfate (PDS): formation of oxidation products and effect of bicarbonate, Water Res. 118 (2017) 196–207.

[38] M. PurnachanderRao, P. Sathishkumar, R.V. Mangalaraja, A.M. Asiri, P. Sivashanmugam, S. Anandan, Simple and low-cost synthesis of CuO nanosheets for visible-light-driven photocatalytic degradation of textile dyes, J. Environ. Chem. Eng., 6 (2018) 2003–2010.

[39] C. Chu, J. Yang, D. Huang, J. Li, A. Wang, P.J.J. Alvarez, J.H. Kim, Cooperative pollutant adsorption and persulfate-driven oxidation on hierarchically ordered porous carbon, Environ. Sci. Technol., 53 (2019) 10352–10360.

[40] Y. Lei, H. Zhang, J. Wang, J. Ai, Rapid and continuous oxidation of organic contaminants with ascorbic acid and a modified ferric/persulfate system, Chem. Eng. J., 270 (2015) 73–79.

[41] Y.F. Rao, L. Qu, H. Yang, W. Chu, Degradation of carbamazepine by Fe(II)-activated persulfate process, J. Hazard. Mater., 268 (2014) 23–32.

[42] X. Wei, N. Gao, C. Li, Y. Deng, S. Zhou, L. Li, Zero-valent iron (ZVI) activation of persulfate (PS) for oxidation of bentazon in water, Chem. Eng. J., 285 (2016) 660–670.

[43] H. Zhang, J. Wang, X. Zhang, B. Li, X. Cheng, Enhanced removal of lomefloxacin based on peroxymonosulfate activation by Co$_3$O$_4$/δ-FeOOH composite, Chem. Eng. J., 369 (2019) 834–844.

[44] L.W. Matzek, K.E. Carter, Sustained persulfate activation using solid iron: kinetics and application to ciprofloxacin degradation, Chem. Eng. J., 307 (2017) 650–660.

[45] A. Ghauch, G. Ayoub, S. Naim, Degradation of sulfamethoxazole by persulfate assisted micrometric Fe^0 in aqueous solution, Chem. Eng. J., 228 (2013) 1168–1181.

[46] L. Yang, L. Xu, X. Bai, P. Jin, Enhanced visible-light activation of persulfate by Ti^{3+} self-doped TiO$_2$/graphene nanocomposite for the rapid and efficient degradation of micropollutants in water, J. Hazard. Mater., 365 (2019) 107–117.

[47] H. Chen, K.C. Carroll, Metal-free catalysis of persulfate activation and organic-pollutant degradation by nitrogen-doped graphene and aminated graphene, Environ. Pollut., 215 (2016) 96–102.

[48] C. Lia, J. Wu, W. Peng, Z. Fang, J. Liu, Peroxymonosulfate activation for efficient sulfamethoxazole degradation by Fe$_3$O$_4$/β-FeOOH nanocomposites: coexistence of radical and non-radical reactions, Chem. Eng. J., 356 (2019) 904–914.

[49] Z.H. Zuo, Z.L. Cai, Y. Katsumura, N. Chitose, Y. Muroya, Reinvestigation of the acid-base equilibrium of the (bi)carbonate radical and pH dependence of its reactivity with inorganic reactants, Radiat. Phys. Chem., 55 (1999) 15–23.

[50] Y. Yang, J.J. Pignatello, J. Ma, W.A. Mitch, Comparison of halide impacts on the efficiency of contaminant degradation by sulfate and hydroxyl radical-based advanced oxidation processes (AOPs), Environ. Sci. Technol., 48 (2014) 2344–2351.

[51] S. Zhu, X. Li, J. Kang, X. Duan, S. Wang, Persulfate activation on crystallographic manganese oxides: mechanism of singlet oxygen evolution for nonradical selective degradation of aqueous contaminants, Environ. Sci. Technol., 53 (2019) 307–315.